National Aeronautics and Space Administration
Research Grant NAG5-12726

Final Report for Research Titled

Aquarius Instrument Science Calibration

During the Risk Reduction Phase

1 December 2004

Covering the period 15 January 2003 through 30 June 2004

Principal Investigator:

Christopher S. Ruf
Department of Atmospheric, Oceanic & Space Sciences
1533 Space Research Building
2455 Hayward
University of Michigan
Ann Arbor, MI 48109-2143
Voice: 734-764-6561
FAX: 734-936-0503
EMail: cruf@umich.edu

Title: Aquarius Instrument Science Calibration During the Risk Reduction Phase
NASA Grant NAG5-12726
Date: 1 December 2004
Prepared by: Christopher S. Ruf (PI)
Department of Atmospheric, Oceanic & Space Sciences
University of Michigan, Ann Arbor
734-764-6561 (V), 734-936-0503 (F), cruf@umich.edu (E)

Table of Contents

Summary of Final Report

This final report presents the results of work performed under NASA Grant NAG5-12726 during the period 15 January 2003 through 30 June 2004. An analysis was performed of a possible vicarious calibration method for use by Aquarius to monitor and stabilize the absolute and relative calibration of its microwave radiometer. Stationary statistical properties of the brightness temperature (T_B) measured by a low Earth orbiting radiometer operating at 1.4135 GHz are considered as a means of validating its absolute calibration. The global minimum, maximum, and average T_B are considered, together with a vicarious cold reference method that detects the presence of a sharp lower bound on naturally occurring values for T_B. Of particular interest is the reliability with which these statistics can be extracted from a realistic distribution of T_B measurements that would be observed by a typical sensor. Simulations of measurements are performed that include the effects of instrument noise and variable environmental factors such as the global water vapor and ocean surface temperature, salinity and wind distributions. Global minima can vary widely due to instrument noise and are not a reliable calibration reference. Global maxima are strongly influenced by several environmental factors as well as instrument noise and are even less stationary. Global averages are largely insensitive to instrument noise and, in most cases, to environmental conditions as well. The global average T_B varies at only the 0.1 K RMS level except in cases of anomalously high winds, when it can increase considerably more. The vicarious cold reference is similarly insensitive to instrument effects and most environmental factors. It is not significantly affected by high wind conditions. The stability of the vicarious reference is, however, found to be somewhat sensitive (at the several tenths of Kelvins level) to variations in the background cold space brightness, T_c. The global average is much less sensitive to this parameter and so using two approaches together can be mutually beneficial.

1. Introduction

The manner in which the microwave brightness temperature (T_B) of the ocean varies as a function of sea surface temperature (SST) and salinity (SSS), near surface wind speed (u) and atmospheric opacity can be taken advantage of as a source of vicarious calibration for an orbiting microwave radiometer. For every microwave frequency, there is an SST and SSS at which the specular T_B of the ocean surface is a minimum. Departures of SST and SSS from that point, as well as all variations in u and atmospheric opacity, will tend to increase the T_B observed by a downward looking radiometer in Earth orbit above its theoretical minimum. An inverse cumulative distribution function (ICDF) for T_B can be constructed which has the property that

$$\text{ICDF}(x) = T_B \quad \text{for } 0 \leq x \leq 1 \tag{1.1}$$

provided x% of the measurements have values below T_B. Given such an ICDF, empirically constructed from T_Bs measured by an orbiting radiometer, the relationship between T_B and x in the range x=1-10% can be extrapolated back to estimate the T_B at which x=0%. This method has been successfully applied to measurements by the TOPEX Microwave Radiometer (TMR) with channels of 18, 21 and 37 GHz at a nadir angle of incidence [Ruf, 2000]. The T_B at which x=0% is found to be repeatable to better than 0.3K over a 6 year period.

Two characteristics of this method of vicarious calibration are important to recognize. First, the conditions for minimum T_B (a specific combination of SST and SSS together with zero winds and a transparent atmosphere) are not ever present, nor do they need to be. It is sufficient that the lower bound on T_B exists and that a significant number of measurements are made in the near vicinity of the minimum. In fact, actual measurements are occasionally recorded below the minimum due to the effects of additive noise and random calibration errors. Extrapolation of the ICDF from a very large set of measurements (in our case covering all of x=1-10%) back to the point x=0% tends to correct for these random effects, provided they are unbiased. (Thus, biased calibration effects can be very quickly identified by this method.) It is much less reliable to simply select a single ICDF value (*e.g.* ICDF at x=0.1%) as a vicarious T_B calibration reference.

A second important characteristic of this method is its ability to adapt to significant changes in the statistical distribution of T_Bs. In the case of TMR, independent ICDFs were derived every 10 days of flight data. Very noticeable changes were observed in the relationship between x and ICDF(x) over the range x=1-10%. This was particularly true of the TMR 21 GHz channel during the 1997-8 ENSO event. The shift in statistics during that period was likely a result of variations in the joint probability of occurrence of SST and atmospheric water vapor. Due to the changes in shape of the ICDF, the extrapolation back to ICDF(x=0%) was performed dynamically by adjusting to the shape of the ICDF independently every 10 days (see Ruf [2000] for details). Thus, while the shape of the ICDF changed significantly during 1997-8, the T_B at which x=0% did not.

Application of the vicarious calibration method to an L-Band radiometer operating at 1.4135 GHz is considered here. The general behavior of T_B versus SST, SSS, polarization and incidence angle are shown in Figures 1.1-1.6. (Details of the forward model used to estimate T_B from the geophysical state are given in Section 2 below.) In each of the figures, the T_B includes only the specular emission component from the ocean surface, together with a water vapor free

atmosphere (assuming O_2 absorption/emission only) and a downwelling cold space brightness of 6K incident on the top of the atmosphere. The effects of atmospheric water vapor and surface wind roughening and foam are neglected here but are considered later. Figures 1.1-1.3 show the dependence of T_Bh (H polarized), T_Bv (V polarized), and T_B1=(T_Bh+T_Bv)/2 (the 1st Stokes polarization) on SST for a typical SSS value of 34 ppt. All three polarizations have maximum T_Bs near SST=15-18C, depending slightly on polarization and incidence angle. Below 15C, T_B decreases monotonically. Sea water in the open ocean has a fairly sharp lower bound at -2C, below which ice forms and T_B increases. The dependence of T_B on SSS is shown in figures 1.4-1.6 at an SST value of -2C. At all incidence angles and polarizations, T_B decreases monotonically with increasing SSS. Thus, the occurrence of minimum T_B will generally coincide with the coldest and saltiest ocean conditions. It is worth noting that the conditions for minimum T_B are independent of incidence angle and are the same for all three polarizations. This is generally not the case at higher microwave frequencies, where the SST that produces a minimum T_B is above $-2\,C$ and varies with both incidence angle and polarization. The fact that a single set of minimum T_B conditions exists should improve the ease with which this technique is applied to Earth orbiting radiometers.

2. Forward Model for Brightness Temperature

The forward model that estimates T_B from the geophysical state is comprised of several components. The dependence of the ocean's complex dielectric constant on SST, SSS and microwave frequency follows the model developed by Stogryn [1997]. This model has a relatively small difference in behavior from those by Klein and Swift [1997] and Ellison et al. [1986] at L-Band. The differences are more pronounced at higher microwave frequencies. The dependence of the ocean surface emissivity on surface wind speed (due to roughening and the presence of foam) is modeled by the following semi-empirical relationship

$$\varepsilon_h = \varepsilon_{h,spec} + u(0.0007 + 0.000015\theta_{inc}) \qquad (2.1)$$
$$\varepsilon_v = \varepsilon_{v,spec} + 0.0007u$$

where ε_p is the emissivity at polarization p, $\varepsilon_{p,spec}$ is the specular component of emissivity at polarization p using Stogryn [1997] for ocean dielectric constant and assuming a perfect (Fresnel) air/sea interface, u is the neutral stability near-surface wind speed, and θ_{inc} is the incidence angle in units of degrees. This model for wind induced excess emissivity follows from Blume *et al.* [1978] for nadir sensitivity, together with an estimated extrapolation to off nadir incidence using a two-scale surface emission model [Wentz, *personal comm.*, 2001].

Atmospheric opacity at L-Band is modeled using the following relationship

$$\tau = (0.009364 + 0.000024127V)\sec(\theta_{inc}) \qquad (2.2)$$

where τ is the line-of-sight opacity through the atmosphere in units of Nepers and V is the zenith integrated water vapor burden present in the atmospheric column in units of cm. The constants in equation (2.2) follow from a regression fit to L-Band opacities derived from a large sample of globally distributed radiosonde profiles over the ocean. Atmospheric upwelling and downwelling brightness are respectively modeled using

$$T_{B,UP} = (1 - e^{-\tau})(SST + 258.15) \qquad (2.3)$$
$$T_{B,DOWN} = (1 - e^{-\tau})(SST + 263.15)$$

where *SST* is in units of Celsius. The relationships between *SST* and the effective upwelling and downwelling atmospheric physical temperature specified in equation (2.3) are based on a similar relationship developed by Wentz [1983].

The total brightness temperature observed from orbit is given by

$$T_B = T_{B,UP} + [(T_c e^{-\tau} + T_{B,DOWN})(1 - \varepsilon_p) + \varepsilon_p (SST + 273.15)]e^{-\tau} \qquad (2.4)$$

where T_c, the cold space background brightness temperature, is taken to be ~6K at L-Band and is varied parametrically in the study described below.

3. Simulation Database

The potential performance of quasi-stationary statistical calibration methods is evaluated by simulating the global distribution of measurements that would be made by an orbiting L-Band radiometer. Global distributions of SST and SSS are provided by NOAA's National Oceanographic Data Center World Ocean Atlas 1998 (WOA98). WOA98 contains (among many other data products) objectively analyzed global fields of SST and SSS on a one-by-one degree grid by season during 1998. The seasons are divided as Winter (January-March), Spring (April-June), Summer (July-September) and Fall (October-December) based on the Northern Hemisphere. Also included are estimates of the standard deviations of SST and SSS during each season and for ea one-by-one degree grid point. The method for objectively analyzing measured data products to produce these gridded fields is described in Levitus *et al.* [1994a,b,c].

Some of the features of the WOA98 average SST and SSS fields are seen in Figures 3.1-3.2, which plot the fields versus latitude during Fall 1998. Coldest SST values (approximately -2 C) appear in both the northern and southern polar regions of Figure 3.1. Highest SSS values within the polar regions (which should combine to yield the lowest specular T_B values) occur in the Southern hemisphere in Figure 3.2. Finally, Figure 3.3 plots SST versus SSS for the Fall 1998 global fields. The cluster of points in the lower right hand corner of the scatter diagram (combining low SST with high SSS) should produce the lowest values of T_B. The WOA98 fields for the standard deviation of SST and SSS have global mean values of 1.03C and 0.25psu, respectively, when grid points without values are ignored. The SST and SSS standard deviations are assumed to equal these average values at grid points without values.

The global distribution of integrated water vapor is also generally dependent on latitude. A simple model for the mean value of this distribution is used of the form

$$V = 1.0 + 3.0\cos(\theta_{LAT}) \qquad (3.1)$$

where V is in unit of cm and θ_{LAT} is the latitude. Equation (3.1) represents the mean value of V. During simulation runs (described in detail below), the value of V is allowed to vary randomly with each realization by assuming a gaussian distribution with standard deviation equal to one half the mean value. The allowed values for V are truncated at V=0.

4. Vicarious Cold Reference T_B Estimator

The minimum, average, and maximum values of T_B derived from a global set of T_B measurements are straightforward statistics. Estimation of the vicarious cold reference statistic is more involved and so is described in detail here. Given an ensemble of T_B measurements (*e.g.* one realization of the simulation runs described below), a vicarious cold reference T_B can be derived by extrapolating the ICDF corresponding to that ensemble back to the T_B with 0% occurrence. The extrapolation is performed by curve fitting a third order polynomial in x to ICDF(x) and then evaluating the polynomial at x=0. Specifically:

1. Sort the T_Bs and compute the value of ICDF(x) at discrete values x=1.0, 1.1, ..., 10.0.

2. Arrange the ICDF into vector form as $\vec{y}$, where y_1=ICDF(1.0), y_2=ICDF(1.1), etc.

3. Define a third order polynomial regression matrix, **P**, by

$$P_{i,j} = (1.0 + 0.1i)^j \tag{4.1}$$

where i = 0, 1, ..., 90 and j = 0, 1, ..., 3.

4. The assumption of a third order polynomial relationship between x and ICDF(x) is equivalent to assuming the model $\vec{y} = \mathbf{P}\vec{c}$, where $\vec{c}$ is a 4-element vector of regression coefficients. The coefficients are found by minimizing the squared error between $\vec{y}$ and $\mathbf{P}\vec{c}$, or

$$\vec{c} = (P^T P)^{-1} P^T \vec{y} \tag{4.2}$$

5. Evaluation of the polynomial approximation to ICDF at x=0% is equivalent to selecting the zeroeth regression coefficient. In other words, the vicarious cold reference T_B equals c_0.

5. T_B Simulations and Sensitivity Studies

Numerous simulations were run to assess the statistical calibration methods. Each realization of the simulation consists of the generation of a global distribution of T_B measurements that could be expected by a low Earth orbiting L-Band radiometer under specified conditions. Simulations were performed independently at off-nadir incidence angles of 0, 20 and 40 degrees and for cases of vertical, horizontal, and 1st Stokes linear polarizations.

The conditions were varied in numerous ways to assess their impact on the stability of the statistics. Potential calibration statistics considered include the minimum, average, maximum and vicarious cold reference. The nominal conditions for the simulations are:

1. T_B measurements are free of biases due to calibration errors. Calibration biases are generally easily identified by vicarious cold reference calibration and would then be removed.

2. T_B measurements are corrupted by zero mean additive gaussian noise with a standard deviation (ΔT) of 2.0 K.

3. The background cold space brightness temperature downwelling onto the top of the atmosphere, T_c, is assumed to be gaussian distributed with a mean value of 6.0 and a standard deviation of 0.6K. Individual realizations that fall below 2.7K are truncated there. Each individual calculation of the T_B measured by the radiometer includes an independent realization of T_c.

4. Near surface wind speed, u, (as it affects the ocean emissivity) is assumed to be uniformly distributed between 0 and 20 m/s. Each individual calculation of the T_B measured by the radiometer includes an independent realization of u.

5. Integrated water vapor burden, V, in the atmosphere is assumed to be gaussian distributed with a mean value given by equation (3.1) and a standard deviation equal to one half the mean. The allowed values for V are truncated at V=0. Each individual calculation of the T_B measured by the radiometer includes an independent realization of V.

6. Global distributions of SST and SSS follow the WOA98 fields. Both variables are assumed to be gaussian distributed with mean values and standard deviations specified by the corresponding WOA98 databases. Each individual calculation of the T_B measured by the radiometer includes an independent realization of SST and SSS. At each lat/lon point on the one-by-one degree grid, 10 independent realizations of T_B are generated.

In all sensitivity studies except the second one described below (Section 5.2), only the Fall 1998 WOA98 data base is used.

5.1. Accuracy of Numerical Simulations

The accuracy with which changes in the vicarious cold reference can be identified due to varying conditions in the simulation is first assessed by considering the repeatability of the numerical simulations. This is done by repeatedly performing the nominal simulation while varying the software random number seed. The results are summarized in Tables 5.1.1-5.1.3. The results are arranged in three separate tables, one for each of the three incidence angles of 0, 20 and 40 degrees. Each table includes results at all three polarization. (All three polarization results at 0 degrees incidence angle should be the same and any differences can be considered another test of the repeatability of the numerical simulation). The statistical results derived from the global ensemble of simulated T_B measurements are arranged as rows in the tables, including the vicarious cold reference value and the minimum, average and maximum values of the T_B distribution.

Ten trials were performed of the simulation and the average and standard deviation of the results over those trials are listed in the tables. The average value of T_B is most repeatable, with standard deviations significantly below 0.01K. Thus, changes in the average T_B due to changing

conditions will be most accurately identified by the following sensitivity studies. The vicarious cold reference value is repeatable at the ~0.02K level for all angles of incidence. The minimum and maximum T_B values are significantly less repeatable, with standard deviations as large as 2K. This is to be expected, given the large number of coupled random perturbations to T_B that are being applied. The magnitude of individual "outlier" T_B values can vary significantly depending on the particular random numbers that are used by the simulator. Note also that the estimates of the vicarious and average standard deviations closely agree between polarizations at 0 degrees incidence, indicating that the estimates of the repeatability are themselves accurate.

5.2. Sensitivity to Season

The effect of season on stability of was assessed by independently performing the simulations at each of the four WOA98 seasonal databases. The results are summarized in Tables 5.1.1-5.1.3. Columns of the tables correspond to the results for individual seasons. In general, it is desirable for the T_B statistics to be unchanged between columns. These results indicate that both the vicarious and average T_Bs are insensitive to seasonal changes in global climatology at the level of a few hundredths of Kelvins.

5.3. Sensitivity to Latitude Band

The dependence of the vicarious cold reference on geographical region was assessed by performing the simulations over: 1) the southern hemisphere only, 2) the mid-latitudes (45S to 45N) only; 3) the northern hemisphere only; and 4) all latitudes together. The results for average T_B indicate a statistically significant lowering of average T_B levels in the southern hemisphere. The difference in average T_B between northern and southern hemisphere results ranges between ~0.2-03K versus incidence angle and polarization. This is consistent with the results presented in Sections 1 and 3 above. The cold, high salinity southern polar regions tend to produce lower T_Bs than their northern polar counterparts. The vicarious cold reference T_B is less sensitive to this characteristic difference between hemispheres. Differences between the northern and southern hemisphere results are at most 0.1K and generally considerably lower. This relative insensitivity results because the 0% extrapolation procedure effectively adjusts to variations in the statistical T_B distribution between hemispheres.

5.4. Sensitivity to Range of SST

A second, surrogate, test of sensitivity to geographic region was performed by comparing the results using all SST values to those using only SSTs below +10C. This effectively combines both northern and southern high latitude bands. The intent is to assess the effects of including the larger variations in joint statistics of SST and SSS present in the north. At the lower angles of incidence, average T_B values shift down by ~0.2K between all-SST and cold-SST cases. At 40 deg incidence, the T_Bv and T_Bl averages decrease by 0.4-0.5K. In general, V-pol T_Bs at higher angles of incidence tend to become increasing sensitive to the physical temperature of the surface (as emissivity increases), and so the greater sensitivity of the average T_B to this SST screening is to be expected. A similarly large shift in average T_B can be seen with the results in Table 5.3.3, where

higher SST values are isolated in the mid-latitude case. The vicarious cold reference T_Bs are less sensitive to the SST screen. Shifts in vicarious T_B are all in the neighborhood of or less than 0.1K.

5.5. Sensitivity to Atmosphere Water Vapor Burden

Sensitivity to the level of atmospheric water vapor was assessed by doubling the mean water vapor burden assumed in the simulation, or

$$V = 2.0 + 6.0\cos(\theta_{LAT}) \tag{5.1}$$

where V is in units of cm and θ_{LAT} is the latitude. The standard deviation of V (equal to one half the mean in the nominal simulation) was assumed to double as well. The results presented in Tables 5.5.1-5.5.3 suggested that water vapor burden has only a very small impact on the stability of either the vicarious or average T_B values. Changes in either are well below 0.1K in all cases.

5.6. Sensitivity to Ocean Surface Winds

The nominal variation in near surface wind speed is assumed to be uniformly distributed between 0 and 20 m/s. (This is a fairly conservative model, from the perspective of evaluating vicarious calibration stability, because it introduces considerably more variation into the T_B ensemble than would a more realistic Rayleigh distributed model.) The dependence of the vicarious cold reference on the wind conditions is assessed by considering a case where wind is uniformly distributed between 0 and 30 m/s. This would, for example, address the validity of this calibration approach during a period of time with anomalously stormy weather on a global scale. The results in Tables 5.6.1-5.6.3 show a clear and statistically significant effect on both vicarious and average T_B levels. Vicarious T_B levels are increased by 0.3-0.4K due to the higher wind conditions. Average T_B levels are increased by 1.0-1.8K. Two points concerning these results are noteworthy. First, significant storm activity, particularly in the higher latitude regions that contribute most to the ICDF at low probabilities of occurrence, can alter the vicarious cold reference by a magnitude likely unacceptable to a climatological salinity mission. Second, the globally averaged T_B is much more significantly affected by anomalously high wind conditions. This greater sensitivity should, however, be qualified by noting that a global scale increase in winds would be required to have such a large effect on the globally averaged T_B whereas a more regional increase in winds near the low SST/high SSS locations would be sufficient to impact the vicarious cold reference.

5.7. Sensitivity to Variability of Cold Space Brightness

The nominal model for the cold space brightness temperature downwelling onto the top of the atmosphere, T_c, is gaussian distributed with a mean value of 6.0 and a standard deviation of 0.6K. The dependence of the vicarious cold reference on T_c is assessed by considering a case where the standard deviation is increased to 1.2K. The results in Tables 5.7.1-5.7.3 show a strong effect on the vicarious cold reference but not on the average T_B. Vicarious T_B is lowered by ~0.2-0.3K with the increased variability in T_c. Average T_B, on the other hand, is hardly affected at all, with changes of a few hundredths of Kelvins at most. The effect on the vicarious cold reference follows from its emphasis on the coldest T_Bs present in the database. Variations in T_C about its

mean value of 6.0K are unbiased. However, the 0% extrapolation procedure effectively weights the realizations of T_C that are below 6.0K more heavily than those that are above it, thus forcing the 0% extrapolation point lower. The average T_B, on the other hand, weights variations in T_C in an unbiased way and is largely unaffected.

The sensitivity to T_C has several ramifications. If the intent of the vicarious calibration method is to provide an absolute calibration reference, then it is necessary to be able to predict what the vicarious cold reference T_B value is. That, in turn, requires that the T_c values in the vicinity of the cold SST/high SSS regions of the world be well known. If vicarious calibration is intended to provide a long term reference against which to validate instrument stability (*i.e.* relative calibration stability as opposed to absolute calibration accuracy), then the sensitivity to variations in T_C could degrade the stationarity of the cold reference. For example, the region of the Earth with lowest T_B measurements may shift significantly from one period to the next. This could occur, for example, because of shifting surface wind fields. The T_C that generally corresponds to each region may differ due to its location relative to the galactic plane, the radiometer viewing geometry, etc. The vicarious cold reference T_B that would be produced in these two cases would be affected. In either case --absolute or relative calibration-- it may be necessary to include a correction for T_C variations in the vicarious cold reference level.

5.8. Sensitivity to Variability of SSS and SST

The standard deviations of the average SST and SSS fields used in the nominal simulations are provided as a WOA98 data product. Average standard deviations over the full global field are 1.03C and 0.25psu. The dependence of the vicarious cold reference on the level of SST and SSS variability is tested by considering a case with twice the WOA98 variability. The results in Tables 5.8.1-5.8.3 show that, while the minimum T_Bs have been very significantly lowered and the maximum T_Bs moderately increased, the effect on both vicarious and average T_Bs is not significant.

6. Effects of Sample Size - Data Record Length Requirements

The simulation results presented in Section 5 all assume that 10 independent measurements are made at each 1x1 deg grid in latitude and longitude over the globe. This would, for example, be roughly consistent with data accumulated over a time sufficient to image the entire Earth by a sensor having three independent cross track samples of 30 km resolution each at a single incidence angle. The dependence of the stability of the global average and vicarious cold reference on sensor type and record length is addressed by considering two specific sensor designs. The SMOS sensor has roughly 40 km cross track by 20 km along track spatial resolution, a swath width of 560 km, and a per sample ΔT of 2.0K. This results in 14 independent cross track samples every 20 km of along track motion, which produces approximately 70 independent samples for every one deg change in latitude due to orbital motion. The Aquarius sensor, an L-Band radiometer design study by NASA Goddard and JPL, makes a single independent measurement every 28 km of along track motion with a ΔT of 0.06K. This results in approximately 3 independent samples per 1 deg change in latitude. Thus, the SMOS sensor has ~23 times more samples but each of its sample is ~33 times noisier. The effects of these two competing features are evaluated here.

The effect of record length on the vicarious calibration stability is modeled by selecting subsets of the full 180x360 deg global grid for processing. Using the complete set of grid points corresponds to the case of full Earth coverage. In a single day for typical low Earth orbits, roughly 14 complete orbit revolutions will be made. In terms of the global grid of SST and SSS data, this corresponds to sampling the grid over all latitudes but in increments of approximately 13 deg in longitude. This results in a subset of the global grid with 12 deg gaps in longitude and 0 deg gaps in latitude. Similarly, a two day record length could be represented by a subset with 6 deg gaps in longitude, etc. (The exact correspondence between record length and longitude gap size depends more precisely on orbit inclination and altitude, but this approximation is sufficient for illustrative purposes.) Numerical simulations were performed in which a subset of the global grid was used. The subset is specified by the gap size in longitude. For a given gap size, a complete set of T_Bs was simulated according to either the SMOS or Aquarius design parameters. The global average and vicarious cold reference T_Bs were then computed. This was repeated 100 times (each time randomly selecting the lowest longitude in the subset to be between one degree and the gap size). The standard deviation of the 100 average and vicarious cold reference T_Bs represents the stability of the reference for the specified sensor type and record length. The results are summarized in Figures 6.1-6.4.

Figure 6.1 shows the stability of the SMOS 1st Stokes brightness vicarious cold reference estimate for varying record lengths. The results for this and all of the following stability tests were similar at horizontal and vertical linear polarization. Using a one day record length (corresponding to 12 deg gaps in longitude coverage), the cold reference has a ~0.1K standard deviation. The stability improves to ~0.05K using a two day record (6 deg gaps) and continues to drop with lengthening time record, reaching 0.01-0.02K with full Earth coverage. This behavior can be interpreted in terms of its impact on potential operational use of the cold reference by considering the variability due to record length as one component of a comprehensive accuracy budget which accounts for all sources of variability. For example, if the most stable calibration reference possible is desired then full Earth coverage should be included in the data set. In this case, the 0.01-0.02K stability predicted in Figure 6.1 would likely only be a small component of the total accuracy budget. Variations due to high wind speeds or changes in T_C may well dominate the error budget in this case. If, on the other hand, daily estimates of the cold reference are needed then the overall accuracy budget could be significantly impacted by the 0.1K stability predicted in Figure 6.1. Such a degraded accuracy budget might be justified if, for example, the on board sensor calibration standards tended to drift on time scales of one day to a greater extent than the overall accuracy of the cold reference. The cold reference could, then, be used to calibrate the on board standards on a daily schedule and the on board standards would be used to calibrate the raw T_B measurements on shorter time scales.

Figure 6.2 shows the stability of the SMOS global average T_B for varying record lengths. This statistic is extremely stable even with short (daily or sub-daily) record lengths. It is likely that a comprehensive accuracy budget for the average T_B would be dominated by other sources of variation with one day or even shorter records. The other sources of variation should, then, be given paramount consideration when deciding what record length to use. For example, while record lengths of less than one day may have more than adequate sample size to guarantee repeatability of the average statistic, they are also more likely to include anomalous weather conditions that can impact the average statistic since anomalies tend to have short time scales.

Figures 6.3 and 6.4 show stability results using the Aquarius sensor parameters. The results are qualitatively similar to those for SMOS but differ markedly in magnitude. The Aquarius cold reference standard deviation is roughly three times that of SMOS. The Aquarius global average T_B is roughly twice as variable versus record length. Recall that SMOS had 33 times the noise and only 23 times the number of samples. If the stability of these statistics were driven simply by the noise in each sample, then SMOS would be more variable by roughly $33/23^{1/2} \approx 7$. In fact, it is two to three times less variable. These results suggest that, in both the cold reference and average T_B cases, a large number of independent realizations of the geophysical state is much more beneficial than is a very low noise floor on each individual realization.

7. Conclusions and Discussion

A simulator has been developed to assess the sensitivity of the vicarious cold reference and global average T_B to variations in numerous environmental factors that alter the statistical distribution of T_Bs that would be measured by an Earth viewing L-Band radiometer. It is found that the globally averaged T_B is relatively insensitive (effected at or below the ~0.1K level) to changes in season, water vapor burden, cold space brightness, and SSS and SST variability. The vicarious cold reference T_B is similarly insensitive to season, water vapor burden and SSS and SST variability, as well as to the selective filtering of data by northern vs. southern hemisphere and by cold vs. all SST values.

The globally averaged T_B shifts by 0.2-0.3K (depending on incidence angle and polarization) when averaged individually over northern versus southern hemispheres. Selectively filtering out only the coldest SST values (below +10.0C) has negligible effect on the average T_B except at vertical and the 1st Stokes polarizations with higher (*e.g.* 40 degrees) angles of incidence. In those cases, the average T_B increases by ~0.4K. Increasing the distribution of near surface wind speeds has a dramatic effect on the globally averaged T_B. A 50% increase in the globally distributed wind speed produces a 1.0-1.8K increase in the average.

The vicarious cold reference is also affected by increases in the wind speed distribution, although to a lesser extent. A 50% increase in wind speed results in a 0.3K increase in the cold reference. It should be noted that the vicarious cold reference can be affected even if the increase in wind speed is confined to isolated regions of the Earth (*e.g.* those with lowest SST and highest SSS values which produce the lowest specular surface T_B measurements). Such a regional increase in wind speeds is probably more likely to occur than is the global increase that would be needed to produce the 1.0-1.8K increase in globally averaged T_B. The vicarious cold reference is much more affected by variations in the background cold space brightness, T_c, than is the global average. A decrease in the vicarious reference by 0.3K results from an increase in RMS variability of T_c from 0.6K to 1.2K about an assumed mean value of 6.0K. This sensitivity suggests that a correction to the vicarious cold reference may be needed in practice if the distribution of background T_c values that are present during the coldest T_B observations changes appreciably.

The fact that the globally averaged and vicarious cold reference T_B statistics tend to vary for different reasons --high winds and varying T_c, respectively-- suggests that using both statistics as calibration references should be mutually beneficial. Potential drifts in on-board sensor calibration

constants would ideally be identified by consistent comparisons against both statistics. If the two statistics indicated different sensor drifts, then the quality of the T_B ensemble from which the statistics were derived could be examined in greater detail. In the case of the global average T_B, the globally averaged wind speed over the period of the data record could be estimated from numerical weather fields and compared to its typical value. The average wind speed over restricted regions with low SST and high SSS could also be used to assess its impact on the vicarious cold reference. The low SST/high SSS regions could also be examined with regard to the average and standard deviation of T_c values observed by the sensor in a specular direction. Significant variations of these T_c statistics would indicate potential variations in the cold reference statistic.

The size of the data ensemble that is required to estimate reliable statistics was also examined. The global average T_B is found to require a considerably smaller data sample than does the vicarious cold reference. Daily accumulations of data are more than sufficient to eliminate sample size as a source of variation in the global average, whereas vicarious cold references that are derived daily will include a component of variability due to sample size that is roughly comparable to other sources of variation in the statistic due to natural geophysical variability.

8. References

Blume A, B.M. Kendall and J.C. Fedors, "Measurements of ocean temperature and salinity via microwave radiometry," *J. Boundary-Layer Meteorology*, **13**, 295, 1978.

Ellison, W. J., A. Balana, G. Delbos, K. Lamkaouchi, L. Eymard, C. Guillou and C. Pringent, "Study and Measurement of the Dielectric Properties of Sea Water," CETP/CNRS, France, ESTEC/Contract 11197/94/NL/CN, Dec. 1996.

Klein, L. A., and C. T. Swift, "An Improved Model for the Dielectric constant of Sea Water at Microwave Frequencies," *IEEE Trans. Antennas Propagat.*, **25**(1), 1977.

Levitus, S., R. Gelfeld, T.P. Boyer, and D. Johnson, "Results of the NODC and IOC Oceanographic Data Archaeology and Rescue Project: Report 1," 64 pp., 1994.

Levitus, S., R. Burgett, and T.P. Boyer, "World Ocean Atlas 1994, Volume 3: Salinity," NOAA Atlas NESDIS 3, 111 pp., 1994.

Levitus, S. and T.P. Boyer. "World Ocean Atlas 1994, Volume 4: Temperature," NOAA Atlas NESDIS 4, 129pp, 1994.

Ruf, C.S. "Detection of calibration drifts in spaceborne microwave radiometers using a vicarious cold reference," *IEEE Trans. Geosci. Remote Sens.*, **38**(1), 44-52, 2000.

Stogryn, A., "Equations for the permittivity of sea water," Naval Research Laboratory Technical Report, Code 7113, PO 570122, 11 pp, 14 Aug 1997.

Wentz, F. J., A model function for ocean microwave brightness temperatures, *J. Geophys. Research*, **88**(C3), 1892-1908, 1983.

9. Tables and Figures

Table 5.1.1. Vicarious Calibration T_B Statistics - Repeated trials at 0 deg incidence, Fall 1998, all latitudes, nominal conditions		
	average of 10 trials	standard deviation of 10 trials
Vicarious T_Bh	95.44	0.016
Min T_Bh	90.04	0.916
Avg T_Bh	101.64	0.007
Max T_Bh	120.34	1.140
Vicarious T_Bv	95.44	0.016
Min T_Bv	90.06	1.178
Avg T_Bv	101.64	0.005
Max T_Bv	121.00	1.284
Vicarious T_B1	95.44	0.016
Min T_B1	88.01	1.118
Avg T_B1	101.64	0.007
Max T_B1	121.30	1.011

Table 5.1.2. Vicarious Calibration T_B Statistics - Repeated trials at 20 deg incidence, Fall 1998, all latitudes, nominal conditions		
	average of 10 trials	standard deviation of 10 trials
Vicarious T_Bh	91.56	0.025
Min T_Bh	85.85	1.641
Avg T_Bh	98.26	0.004
Max T_Bh	117.74	1.232
Vicarious T_Bv	100.56	0.025
Min T_Bv	94.18	1.898
Avg T_Bv	106.43	0.006
Max T_Bv	126.80	1.483
Vicarious T_B1	96.56	0.025
Min T_B1	88.56	1.443
Avg T_B1	102.35	0.005
Max T_B1	122.45	0.907

Table 5.1.3. Vicarious Calibration T_B Statistics - Repeated trials at 40 deg incidence, Fall 1998, all latitudes, nominal conditions		
	average of 10 trials	standard deviation of 10 trials
Vicarious T_Bh	79.37	0.014
Min T_Bh	74.38	0.856
Avg T_Bh	86.64	0.004
Max T_Bh	105.37	2.340
Vicarious T_Bv	116.37	0.015
Min T_Bv	110.37	1.443
Avg T_Bv	123.42	0.007
Max T_Bv	145.34	1.066
Vicarious T_B1	97.37	0.014
Min T_B1	91.69	0.633
Avg T_B1	105.03	0.004
Max T_B1	126.43	1.825

Table 5.2.1. Vicarious Calibration T_B Statistics - 0 deg incidence, all latitudes, nominal conditions				
	Winter 1998	Spring 1998	Summer 1998	Fall 1998
Vicarious T_Bh	95.49	95.45	95.40	95.41
Min T_Bh	90.93	90.86	90.53	88.58
Avg T_Bh	101.64	101.61	101.68	101.63
Max T_Bh	126.33	125.61	126.52	121.69
Vicarious T_Bv	95.49	95.45	95.40	95.41
Min T_Bv	88.76	90.40	90.77	90.78
Avg T_Bv	101.65	101.62	101.69	101.64
Max T_Bv	127.12	124.60	127.32	120.35
Vicarious T_B1	95.49	95.45	95.40	95.41
Min T_B1	85.47	89.14	89.22	88.14
Avg T_B1	101.64	101.61	101.68	101.63
Max T_B1	126.41	126.42	126.60	122.35

Table 5.2.2. Vicarious Calibration T_B Statistics - 20 deg incidence, all latitudes, nominal conditions				
	Winter 1998	Spring 1998	Summer 1998	Fall 1998
Vicarious T_Bh	91.58	91.54	91.55	91.55
Min T_Bh	87.01	84.36	86.67	86.72
Avg T_Bh	98.27	98.24	98.31	98.26
Max T_Bh	120.62	118.54	120.81	118.04
Vicarious T_Bv	100.58	100.54	100.55	100.55
Min T_Bv	94.97	94.17	95.05	95.11
Avg T_Bv	106.44	106.41	106.49	106.44
Max T_Bv	129.62	128.86	129.16	126.94
Vicarious T_B1	96.58	96.54	96.55	96.55
Min T_B1	89.44	89.26	89.47	89.35
Avg T_B1	102.35	102.33	102.39	102.35
Max T_B1	125.58	125.32	125.50	123.34

Table 5.2.3. Vicarious Calibration T_B Statistics - 40 deg incidence, all latitudes, nominal conditions				
	Winter 1998	Spring 1998	Summer 1998	Fall 1998
Vicarious T_Bh	79.40	79.37	79.37	79.36
Min T_Bh	73.22	74.97	74.31	73.02
Avg T_Bh	86.64	86.61	86.67	86.64
Max T_Bh	106.13	107.27	106.23	102.84
Vicarious T_Bv	116.40	116.37	116.37	116.36
Min T_Bv	111.40	110.81	112.60	111.24
Avg T_Bv	123.43	123.39	123.47	123.42
Max T_Bv	149.35	148.29	149.56	144.73
Vicarious T_B1	97.40	97.37	97.37	97.36
Min T_B1	88.35	91.80	89.81	88.17
Avg T_B1	105.03	105.00	105.07	105.02
Max T_B1	129.73	129.71	129.92	125.30

Table 5.3.1. Vicarious Calibration T_B Statistics - 0 deg incidence, selected latitudes, Fall 1998, nominal conditions				
	Southern Hemisphere	Mid latitudes (45S to 45N)	Northern Hemisphere	All latitudes
Vicarious T_Bh	95.41	95.50	95.46	95.41
Min T_Bh	90.27	90.73	91.06	88.58
Avg T_Bh	101.55	101.78	101.73	101.63
Max T_Bh	121.03	121.23	121.41	121.69
Vicarious T_Bv	95.41	95.50	95.46	95.41
Min T_Bv	90.77	90.63	90.96	90.78
Avg T_Bv	101.56	101.79	101.74	101.64
Max T_Bv	123.05	122.77	119.72	120.35
Vicarious T_B1	95.41	95.50	95.46	95.41
Min T_B1	90.02	90.08	90.10	88.14
Avg T_B1	101.56	101.79	101.73	101.63
Max T_B1	120.95	122.22	124.10	122.35

Table 5.3.2. Vicarious Calibration T_B Statistics - 20 deg incidence, selected latitudes, Fall 1998, nominal conditions				
	Southern Hemisphere	Mid latitudes (45S to 45N)	Northern Hemisphere	All latitudes
Vicarious T_Bh	91.47	91.59	91.57	91.55
Min T_Bh	87.58	87.35	87.74	86.72
Avg T_Bh	98.17	98.40	98.35	98.26
Max T_Bh	117.89	120.26	116.09	118.04
Vicarious T_Bv	100.47	100.59	100.57	100.55
Min T_Bv	95.60	95.87	95.79	95.11
Avg T_Bv	106.35	106.64	106.55	106.44
Max T_Bv	126.55	124.04	126.09	126.94
Vicarious T_B1	96.47	96.59	96.57	96.55
Min T_B1	89.73	89.24	90.10	89.35
Avg T_B1	102.25	102.51	102.45	102.35
Max T_B1	122.89	121.60	123.63	123.34

Table 5.3.3. Vicarious Calibration T_B Statistics - 40 deg incidence, selected latitudes, Fall 1998, nominal conditions

	Southern Hemisphere	Mid latitudes (45S to 45N)	Northern Hemisphere	All latitudes
Vicarious T_Bh	79.30	79.41	79.37	79.36
Min T_Bh	74.04	74.92	75.14	73.02
Avg T_Bh	86.58	86.79	86.73	86.64
Max T_Bh	102.03	103.75	104.15	102.84
Vicarious T_Bv	116.30	116.41	116.37	116.36
Min T_Bv	113.01	112.81	112.81	111.24
Avg T_Bv	123.33	123.82	123.56	123.42
Max T_Bv	143.97	144.35	144.74	144.73
Vicarious T_Bl	97.30	97.41	97.37	97.36
Min T_Bl	91.42	91.87	92.95	88.17
Avg T_Bl	104.95	105.31	105.15	105.02
Max T_Bl	123.40	125.63	124.59	125.30

Table 5.4.1. Vicarious Calibration T_B Statistics - 0 deg incidence, Fall 1998, all latitudes, filtered by SST

	Full SST range (-2 to +31C)	Cold SSTs (-2 to +10 C)
Vicarious T_Bh	95.41	95.34
Min T_Bh	88.58	90.59
Avg T_Bh	101.63	101.43
Max T_Bh	121.69	116.95
Vicarious T_Bv	95.41	95.34
Min T_Bv	90.78	90.73
Avg T_Bv	101.64	101.44
Max T_Bv	120.35	114.80
Vicarious T_Bl	95.41	95.34
Min T_Bl	88.14	89.88
Avg T_Bl	101.63	101.43
Max T_Bl	122.35	116.37

Table 5.4.2. Vicarious Calibration T_B Statistics - 20 deg incidence, Fall 1998, all latitudes, filtered by SST		
	Full SST range (-2 to +31C)	Cold SSTs (-2 to +10 C)
Vicarious T_Bh	91.55	91.44
Min T_Bh	86.72	87.50
Avg T_Bh	98.26	98.05
Max T_Bh	118.04	110.38
Vicarious T_Bv	100.55	100.44
Min T_Bv	95.11	96.00
Avg T_Bv	106.44	106.18
Max T_Bv	126.94	120.14
Vicarious T_B1	96.55	96.44
Min T_B1	89.35	89.58
Avg T_B1	102.35	102.11
Max T_B1	123.34	116.99

Table 5.4.3. Vicarious Calibration T_B Statistics - 40 deg incidence, Fall 1998, all latitudes, filtered by SST		
	Full SST range (-2 to +31C)	Cold SSTs (-2 to +10 C)
Vicarious T_Bh	79.36	79.34
Min T_Bh	73.02	75.10
Avg T_Bh	86.64	86.44
Max T_Bh	102.84	99.70
Vicarious T_Bv	116.36	116.34
Min T_Bv	111.24	112.25
Avg T_Bv	123.42	122.89
Max T_Bv	144.73	137.74
Vicarious T_B1	97.36	97.34
Min T_B1	88.17	92.82
Avg T_B1	105.02	104.66
Max T_B1	125.30	119.89

Table 5.5.1. Vicarious Calibration T_B Statistics - 0 deg incidence, Fall 1998, all latitudes, variable integrated water vapor burden		
	nominal water vapor burden	double water vapor burden
Vicarious T_Bh	95.41	95.44
Min T_Bh	88.58	88.61
Avg T_Bh	101.63	101.66
Max T_Bh	121.69	121.73
Vicarious T_Bv	95.41	95.44
Min T_Bv	90.78	90.79
Avg T_Bv	101.64	101.67
Max T_Bv	120.35	120.40
Vicarious T_Bl	95.41	95.44
Min T_Bl	88.14	88.19
Avg T_Bl	101.63	101.66
Max T_Bl	122.35	122.37

Table 5.5.2. Vicarious Calibration T_B Statistics - 20 deg incidence, Fall 1998, all latitudes, variable integrated water vapor burden		
	nominal water vapor burden	double water vapor burden
Vicarious T_Bh	91.55	91.57
Min T_Bh	86.72	86.75
Avg T_Bh	98.26	98.29
Max T_Bh	118.04	118.07
Vicarious T_Bv	100.55	100.57
Min T_Bv	95.11	95.13
Avg T_Bv	106.44	106.47
Max T_Bv	126.94	126.96
Vicarious T_Bl	96.55	96.57
Min T_Bl	89.35	89.41
Avg T_Bl	102.35	102.38
Max T_Bl	123.34	123.37

Table 5.5.3. Vicarious Calibration T_B Statistics - 40 deg incidence, Fall 1998, all latitudes, variable integrated water vapor burden		
	nominal water vapor burden	double water vapor burden
Vicarious T_Bh	79.36	79.42
Min T_Bh	73.02	73.05
Avg T_Bh	86.64	86.67
Max T_Bh	102.84	102.86
Vicarious T_Bv	116.36	116.42
Min T_Bv	111.24	111.26
Avg T_Bv	123.42	123.45
Max T_Bv	144.73	144.75
Vicarious T_Bl	97.36	97.42
Min T_Bl	88.17	88.20
Avg T_Bl	105.02	105.06
Max T_Bl	125.30	125.37

Table 5.6.1. Vicarious Calibration T_B Statistics - 0 deg incidence, Fall 1998, all latitudes, variable sea surface wind speed		
	nominal wind speed	50% greater wind speed
Vicarious T_Bh	95.41	95.74
Min T_Bh	88.58	88.68
Avg T_Bh	101.63	102.60
Max T_Bh	121.69	123.25
Vicarious T_Bv	95.41	95.74
Min T_Bv	90.78	91.40
Avg T_Bv	101.64	102.61
Max T_Bv	120.35	121.64
Vicarious T_Bl	95.41	95.74
Min T_Bl	88.14	88.19
Avg T_Bl	101.63	102.60
Max T_Bl	122.35	123.25

Table 5.6.2. Vicarious Calibration T_B Statistics - 20 deg incidence, Fall 1998, all latitudes, variable sea surface wind speed		
	nominal wind speed	50% greater wind speed
Vicarious T_Bh	91.55	91.90
Min T_Bh	86.72	86.85
Avg T_Bh	98.26	99.64
Max T_Bh	118.04	120.06
Vicarious T_Bv	100.55	100.90
Min T_Bv	95.11	95.30
Avg T_Bv	106.44	107.40
Max T_Bv	126.94	128.30
Vicarious T_Bl	96.55	96.90
Min T_Bl	89.35	89.60
Avg T_Bl	102.35	103.52
Max T_Bl	123.34	125.06

Table 5.6.3. Vicarious Calibration T_B Statistics - 40 deg incidence, Fall 1998, all latitudes, variable sea surface wind speed		
	nominal wind speed	50% greater wind speed
Vicarious T_Bh	79.36	79.73
Min T_Bh	73.02	73.07
Avg T_Bh	86.64	88.41
Max T_Bh	102.84	105.91
Vicarious T_Bv	116.36	116.73
Min T_Bv	111.24	111.27
Avg T_Bv	123.42	124.38
Max T_Bv	144.73	146.38
Vicarious T_Bl	97.36	97.73
Min T_Bl	88.17	88.21
Avg T_Bl	105.02	106.39
Max T_Bl	125.30	127.65

Table 5.7.1. Vicarious Calibration T_B Statistics - 0 deg incidence, Fall 1998, all latitudes, variable variability in background cold space brightness		
	nominal T_C variability (0.6 K RMS)	double T_C variability (1.2 K RMS)
Vicarious T_Bh	95.41	95.17
Min T_Bh	88.58	89.38
Avg T_Bh	101.63	101.63
Max T_Bh	121.69	122.15
Vicarious T_Bv	95.41	95.17
Min T_Bv	90.78	90.52
Avg T_Bv	101.64	101.64
Max T_Bv	120.35	120.62
Vicarious T_Bl	95.41	95.17
Min T_Bl	88.14	87.46
Avg T_Bl	101.63	101.64
Max T_Bl	122.35	122.55

Table 5.7.2. Vicarious Calibration T_B Statistics - 20 deg incidence, Fall 1998, all latitudes, variable variability in background cold space brightness		
	nominal T_C variability (0.6 K RMS)	double T_C variability (1.2 K RMS)
Vicarious T_Bh	91.55	91.30
Min T_Bh	86.72	86.27
Avg T_Bh	98.26	98.26
Max T_Bh	118.04	117.99
Vicarious T_Bv	100.55	100.30
Min T_Bv	95.11	94.62
Avg T_Bv	106.44	106.44
Max T_Bv	126.94	126.99
Vicarious T_Bl	96.55	96.30
Min T_Bl	89.35	88.69
Avg T_Bl	102.35	102.35
Max T_Bl	123.34	123.29

Table 5.7.3. Vicarious Calibration T_B Statistics - 40 deg incidence, Fall 1998, all latitudes, variable variability in background cold space brightness		
	nominal T_C variability (0.6 K RMS)	double T_C variability (1.2 K RMS)
Vicarious T_Bh	79.36	79.09
Min T_Bh	73.02	72.22
Avg T_Bh	86.64	86.64
Max T_Bh	102.84	103.14
Vicarious T_Bv	116.36	116.09
Min T_Bv	111.24	110.57
Avg T_Bv	123.42	123.42
Max T_Bv	144.73	144.97
Vicarious T_Bl	97.36	97.09
Min T_Bl	88.17	87.44
Avg T_Bl	105.02	105.03
Max T_Bl	125.30	125.56

Table 5.8.1. Vicarious Calibration T_B Statistics - 0 deg incidence, Fall 1998, all latitudes, variable variability from climatology of SSS and SST fields		
	nominal SSS & SST variability	double SSS & SST variability
Vicarious T_Bh	95.41	95.36
Min T_Bh	88.58	80.79
Avg T_Bh	101.63	101.63
Max T_Bh	121.69	126.32
Vicarious T_Bv	95.41	95.36
Min T_Bv	90.78	81.22
Avg T_Bv	101.64	101.64
Max T_Bv	120.35	123.10
Vicarious T_Bl	95.41	95.36
Min T_Bl	88.14	77.93
Avg T_Bl	101.63	101.63
Max T_Bl	122.35	126.49

Table 5.8.2. Vicarious Calibration T_B Statistics - 20 deg incidence, Fall 1998, all latitudes, variable variability from climatology of SSS and SST fields		
	nominal SSS & SST variability	double SSS & SST variability
Vicarious T_Bh	91.55	91.50
Min T_Bh	86.72	81.89
Avg T_Bh	98.26	98.26
Max T_Bh	118.04	118.63
Vicarious T_Bv	100.55	100.50
Min T_Bv	95.11	85.52
Avg T_Bv	106.44	106.44
Max T_Bv	126.94	126.53
Vicarious T_Bl	96.55	96.50
Min T_Bl	89.35	83.05
Avg T_Bl	102.35	102.35
Max T_Bl	123.34	123.72

Table 5.8.3. Vicarious Calibration T_B Statistics - 40 deg incidence, Fall 1998, all latitudes, variable variability from climatology of SSS and SST fields		
	nominal SSS & SST variability	double SSS & SST variability
Vicarious T_Bh	79.36	79.36
Min T_Bh	73.02	68.62
Avg T_Bh	86.64	86.63
Max T_Bh	102.84	105.06
Vicarious T_Bv	116.36	116.36
Min T_Bv	111.24	99.45
Avg T_Bv	123.42	123.42
Max T_Bv	144.73	146.56
Vicarious T_Bl	97.36	97.36
Min T_Bl	88.17	82.83
Avg T_Bl	105.02	105.02
Max T_Bl	125.30	125.64

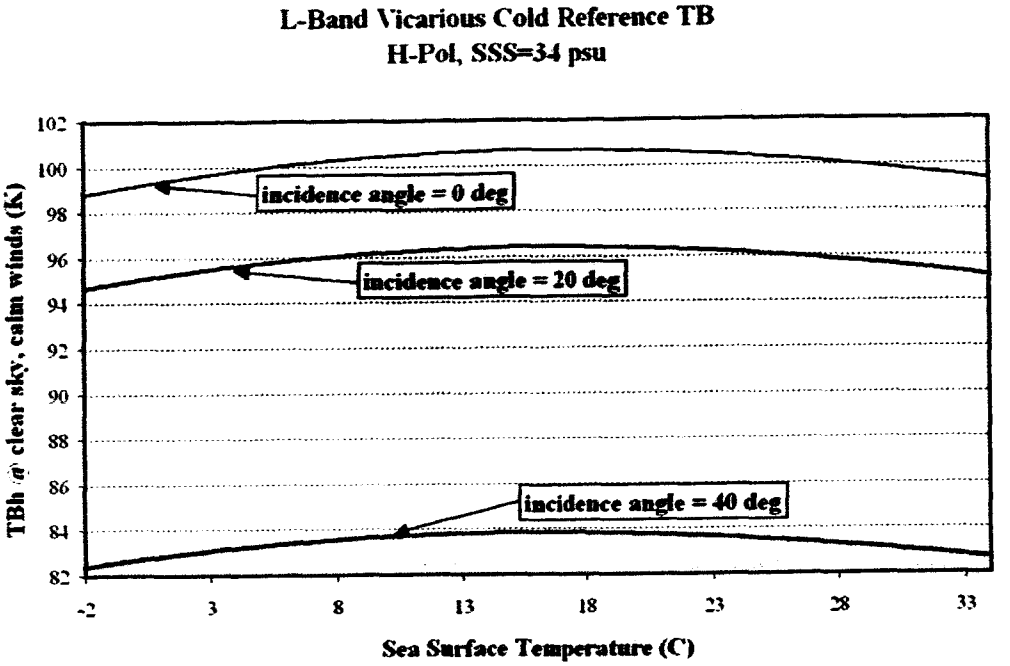

Figure 1.1. Coldest ocean T_B (no water vapor or wind roughening) at 1.4135 GHz, H-pol versus SST and incidence angle.

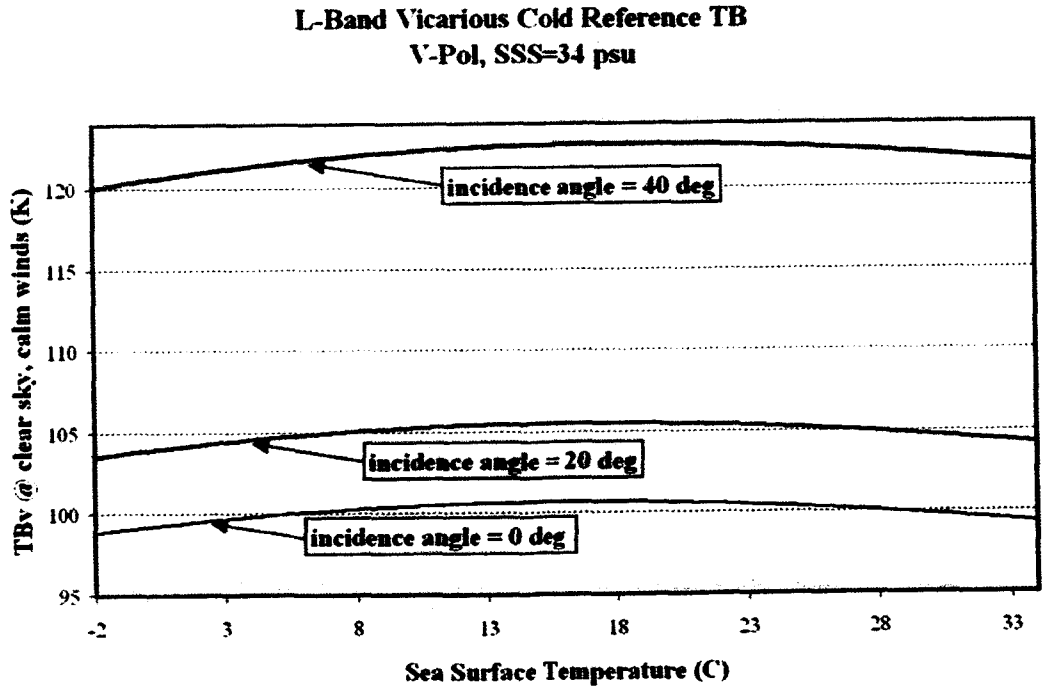

Figure 1.2. Coldest ocean T_B (no water vapor or wind roughening) at 1.4135 GHz, V-pol versus SST and incidence angle.

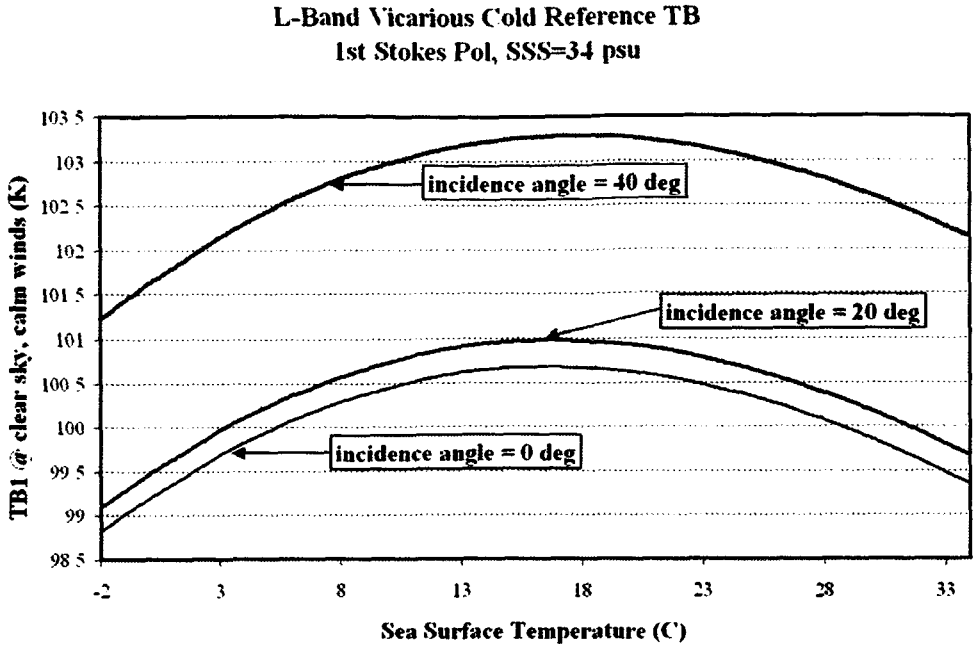

Figure 1.3. Coldest ocean T_B (no water vapor or wind roughening) at 1.4135 GHz, 1st Stokes ($\frac{TB_V + TB_H}{2}$) Pol versus SST and incidence angle.

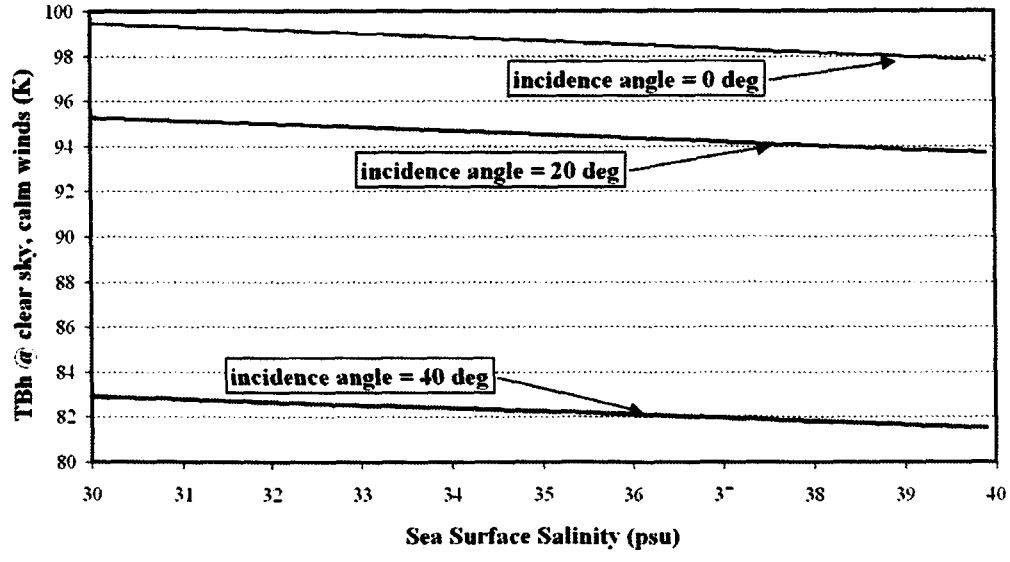

Figure 1.4. Coldest ocean T_B (no water vapor or wind roughening) at 1.4135 GHz, H-pol versus SSS and incidence angle.

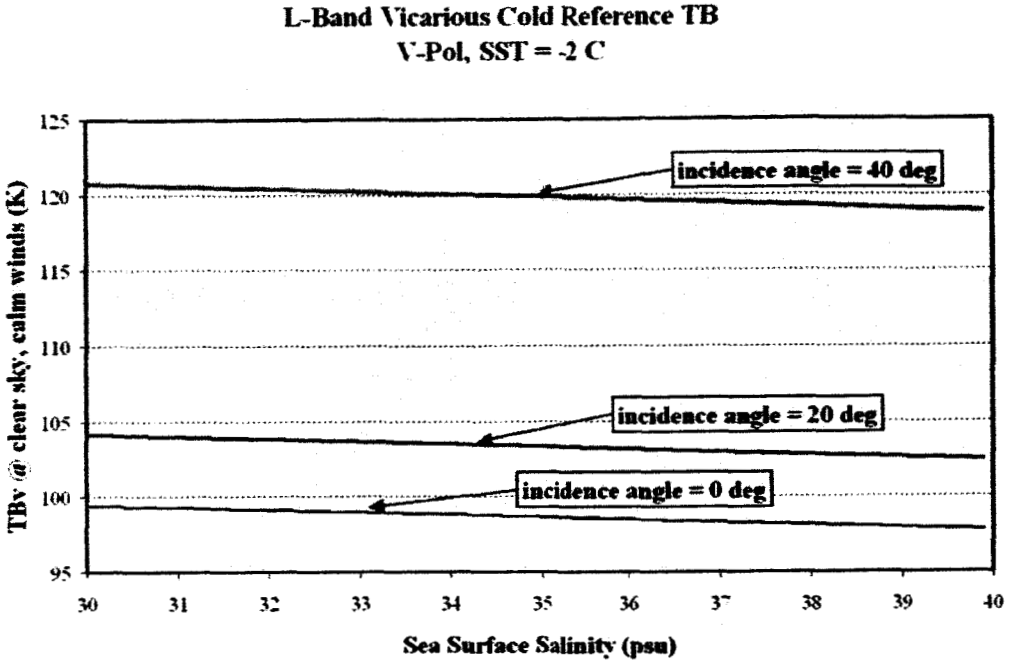

Figure 1.5. Coldest ocean T_B (no water vapor or wind roughening) at 1.4135 GHz, V-pol versus SSS and incidence angle.

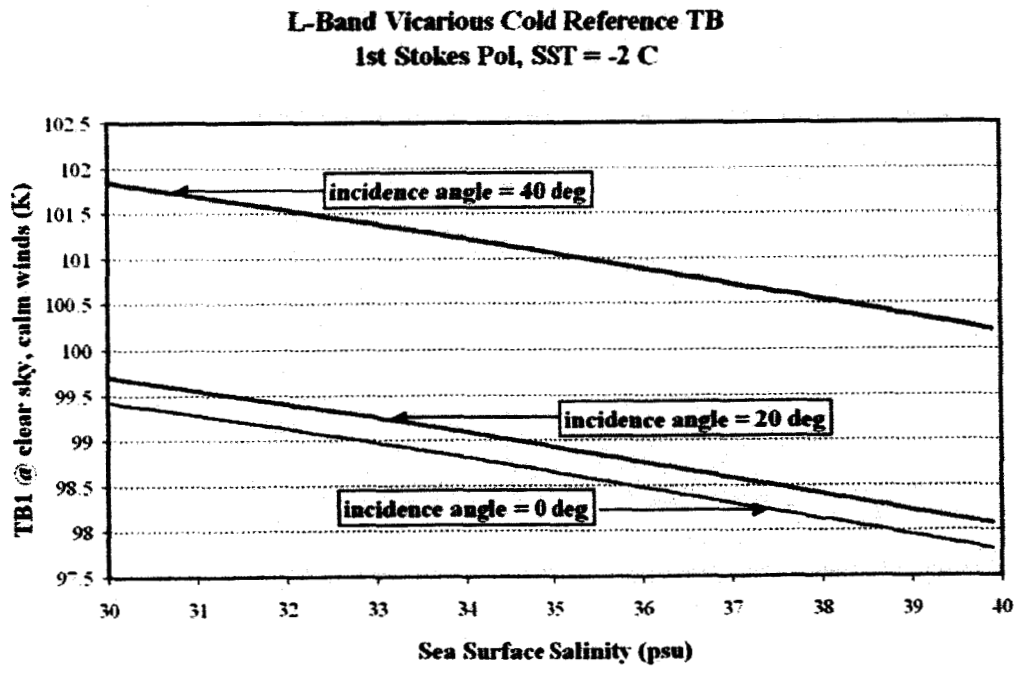

Figure 1.6. Coldest ocean T_B (no water vapor or wind roughening) at 1.4135 GHz, 1st Stokes $(\frac{TB_V + TB_H}{2})$ Pol versus SSS and incidence angle.

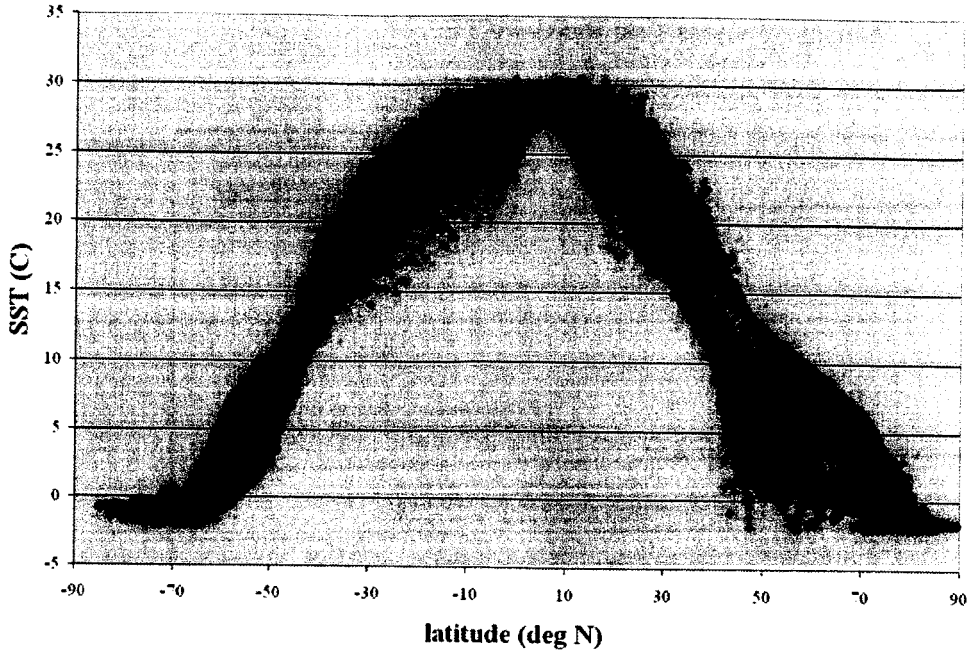

Figure 3.1. SST versus latitude from WOA98 objectively analyzed ocean fields on 1x1 deg grid for Fall 1998.

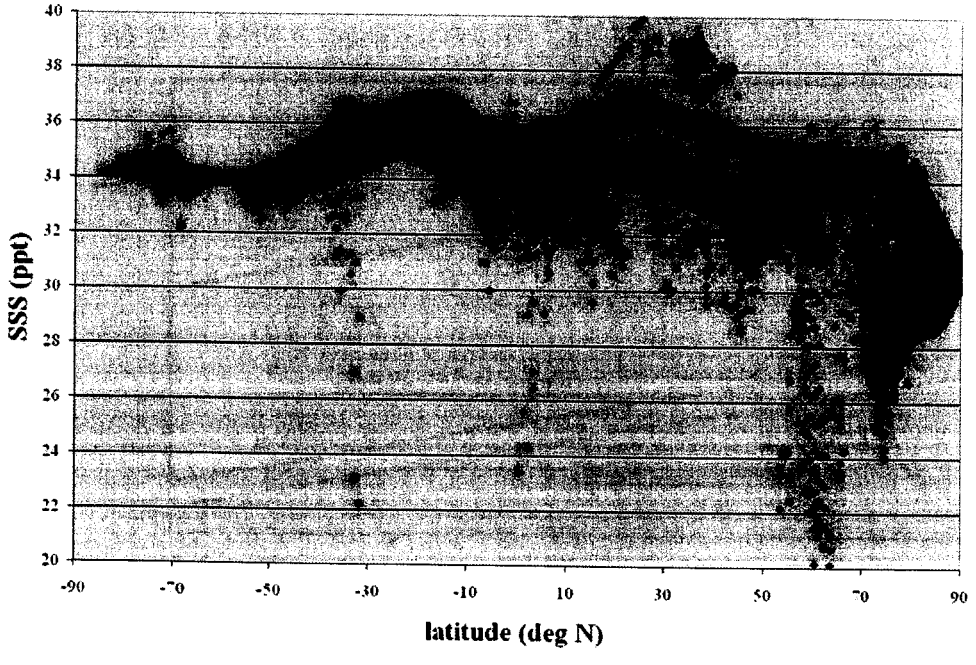

Figure 3.2. SSS versus latitude from WOA98 objectively analyzed ocean fields on 1x1 deg grid for Fall 1998.

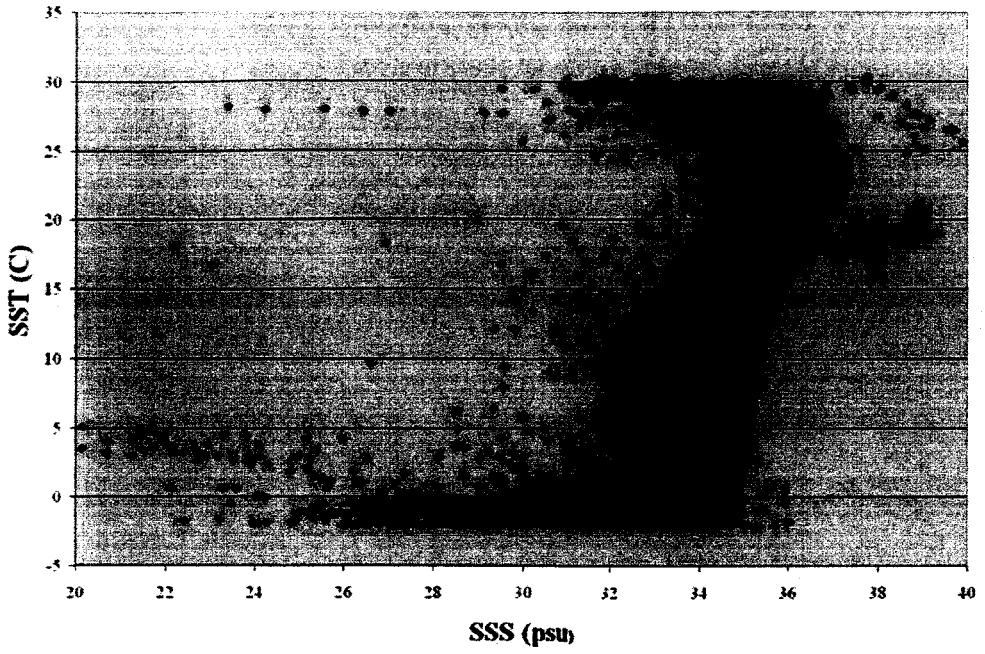

Figure 3.3. SSS versus SST from WOA98 objectively analyzed ocean fields on 1x1 deg grid for Fall 1998.

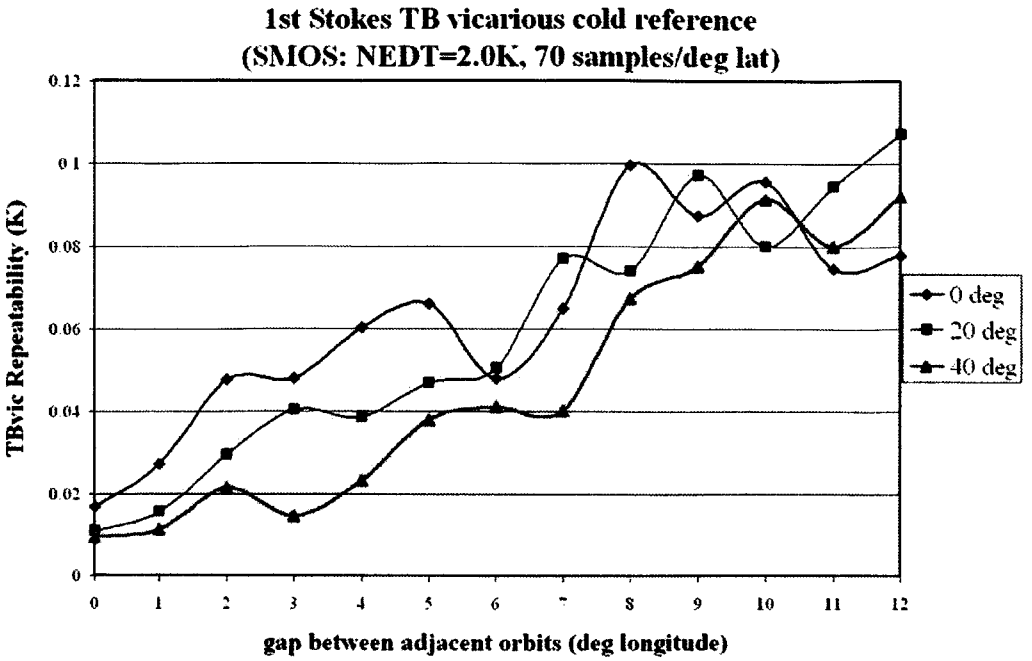

Figure 6.1. Stability of the vicarious cold reference applied to the SMOS sensor parameters versus Earth coverage (or, equivalently, versus data base record length).

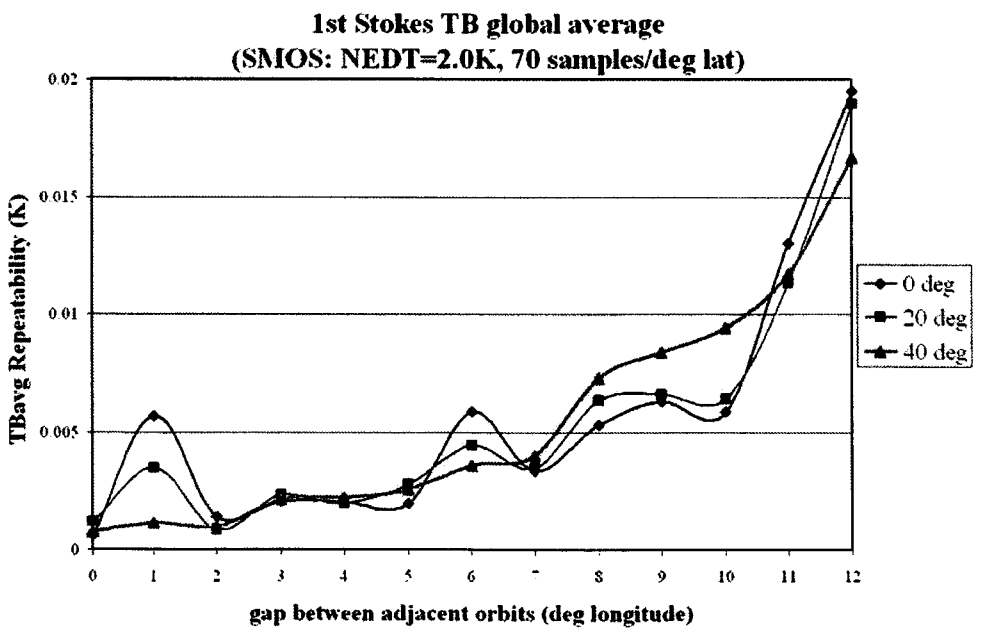

Figure 6.2. Stability of the global average T_B applied to the SMOS sensor parameters versus Earth coverage (or, equivalently, versus data base record length).

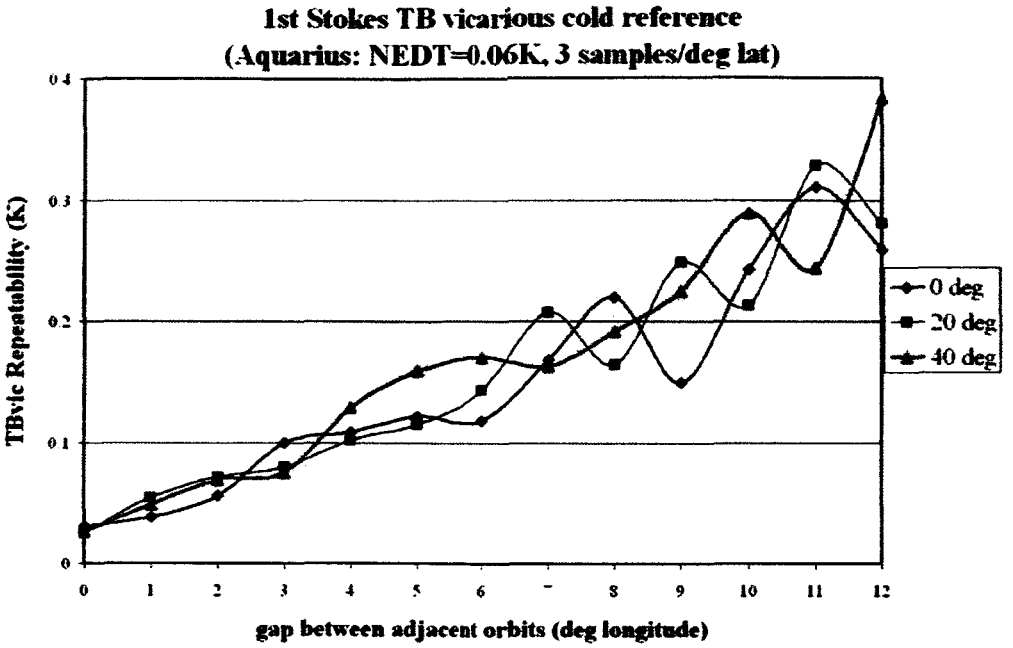

Figure 6.3. Stability of the vicarious cold reference applied to the Aquarius sensor parameters versus Earth coverage (or, equivalently, versus data base record length).

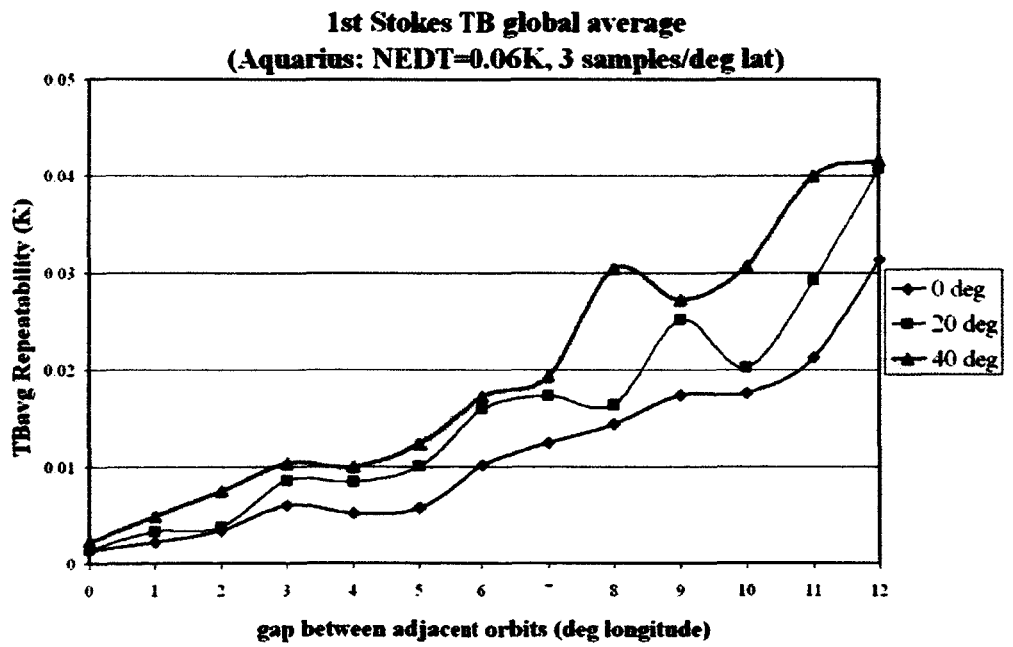

Figure 6.4. Stability of the global average T_B applied to the Aquarius sensor parameters versus Earth coverage (or, equivalently, versus data base record length).

10. Publications generated by this project

Ruf, C.S., "Vicarious Calibration of an Ocean Salinity Radiometer from Low Earth Orbit," AMS J. Atmos. Oceanic Tech., **20**(11), 1656-1670, 2003.